

# RNA polymerase clamp conformational dynamics: long-lived states and modulation by crowding, cations, and nonspecific DNA binding

Abhishek Mazumder<sup>1,\*</sup>, Anna Wang<sup>1</sup>, Heesoo Uhm<sup>1</sup>, Richard H. Ebright<sup>2</sup> and Achillefs N. Kapanidis<sup>1,\*</sup>

<sup>1</sup>Biological Physics Research Group, Clarendon Laboratory, Department of Physics, University of Oxford, Oxford OX1 3PU, UK and <sup>2</sup>Waksman Institute and Department of Chemistry, Rutgers University, Piscataway, NJ 08854, USA

Received October 03, 2020; Revised January 23, 2021; Editorial Decision January 25, 2021; Accepted January 28, 2021

## ABSTRACT

The RNA polymerase (RNAP) clamp, a mobile structural element conserved in RNAP from all domains of life, has been proposed to play critical roles at different stages of transcription. In previous work, we demonstrated using single-molecule Förster resonance energy transfer (smFRET) that RNAP clamp interconvert between three short-lived conformational states (lifetimes  $\sim 0.3$ – $0.6$  s), that the clamp can be locked into any one of these states by small molecules, and that the clamp stays closed during initial transcription and elongation. Here, we extend these studies to obtain a comprehensive understanding of clamp dynamics under conditions RNAP may encounter in living cells. We find that the RNAP clamp can populate long-lived conformational states (lifetimes  $> 1.0$  s) and can switch between these long-lived states and the previously observed short-lived states. In addition, we find that clamp motions are increased in the presence of molecular crowding, are unchanged in the presence of elevated monovalent-cation concentrations, and are reduced in the presence of elevated divalent-cation concentrations. Finally, we find that RNAP bound to non-specific DNA predominantly exhibits a closed clamp conformation. Our results raise the possibility of additional regulatory checkpoints that could affect clamp dynamics and consequently could affect transcription and transcriptional regulation.

## INTRODUCTION

Transcription is the first and most highly regulated step in gene expression (1). The first step of transcription is the formation of the open complex (R<sub>Po</sub>), in which the RNA

polymerase holoenzyme (RNAP) binds to a promoter DNA fragment and unwinds double-stranded DNA, resulting in a  $\sim 12$ – $14$  bp bubble where the individual DNA strands are separated, and single strands of DNA interact with RNAP in a sequence-specific manner (2). Extensive structural studies of RNAP, the R<sub>Po</sub> and initial transcribing complexes (R<sub>Pitc</sub>) reveal that although RNAP accommodates single strands of DNA in the RNAP active-site cleft, access of double-stranded DNA (width  $\sim 20$  Å; (3)) inside the cleft is restricted due to the narrow width of the cleft ( $< 20$  Å) (4–7). This raises the question as to how and when the promoter DNA unwinds on path to the final R<sub>Po</sub>.

One of the prevailing models in the field implicates the RNAP clamp, a structural element that forms one wall of the active-site cleft, as a crucial player in R<sub>Po</sub> formation. According to this model, after initial DNA binding, the clamp can swing open, widening the RNAP active-site cleft; this conformational change licenses entry of duplex DNA, subsequent melting of DNA inside the cleft, and clamp closure, resulting in a catalytically competent R<sub>Po</sub>. Some structural studies have captured the clamp in open clamp conformations that would allow entry of duplex DNA inside the cleft (8). Recent structural studies on a  $\sigma 54$  RNAP-promoter complex also captured a conformation where double-stranded DNA is located inside the RNAP cleft with a wide-open clamp conformation (9). However, it has not been established conclusively that such conformations are on-pathway to R<sub>Po</sub> formation. Additionally, motions of the clamp have been proposed to play crucial roles in transcription elongation (10,11) and transcription termination (12).

It is therefore important to study clamp conformations and conformational dynamics in solution, and in real time, to detect and characterize clamp conformations and conformational dynamics, to determine timescales of the clamp conformational dynamics, to understand the modulation of clamp conformational dynamics by changes in conditions, and to assess the functional relevance of clamp con-

\*To whom correspondence should be addressed. Tel: +44 1865 272 226; Email: a.kapanidis1@physics.ox.ac.uk  
Correspondence may also be addressed to Abhishek Mazumder. Email: abhishek.mazumder@physics.ox.ac.uk

formational dynamics. Clamp conformation and conformational dynamics can be directly detected and characterized using single-molecule FRET (smFRET), which enables measurement of distances, in the range of 2–10 nm, between pairs of fluorophores incorporated at specific sites within a macromolecule (13). One of the major challenges in performing smFRET measurements is the incorporation of a pair of fluorophores at specific sites of interest in the macromolecule of interest. In previous work, we developed a procedure that combines unnatural-amino-acid mutagenesis and Staudinger ligation to enable preparation of RNAP derivatives having the fluorescent probes Cy3B and Alexa 647 incorporated at the tip of the RNAP clamp and the tip of the opposite wall of the RNAP active-site cleft (13,14). We first used the resulting doubly labelled RNAP derivatives to monitor clamp conformations in freely diffusing RNAP molecules in solution through smFRET with confocal alternating laser excitation microscopy (confocal ALEX; 13). We next used the doubly labelled RNAP derivatives to monitor clamp conformational dynamics in surface-immobilized RNAP molecules in solution, *in real time*, through smFRET with total internal reflection fluorescence ALEX microscopy (TIRF-ALEX; 15,16). We observed that, in RNAP holoenzyme, the clamp populates three distinct conformations: an open clamp, a partly closed clamp, and a closed clamp conformation (13,15,16). We also showed that the clamp switches among these three short-lived conformational states on the millisecond time scale and can be trapped in any one of these three conformations by the RNAP inhibitors myxopyronin, coralopyronin, ripostatin, fidaxomicin (lipiarmycin), and ppGppp (13,15,16). Additionally, we observed that the clamp adopts exclusively or nearly exclusively, a closed conformation in the RNAP–promoter open complex (RPo), RNAP–promoter initial transcribing complexes (RPitc) and RNAP–DNA elongation complexes (RDe) (13,15).

Here, we extend our studies to further our understanding of modulation of clamp conformational dynamics in solution in real time under several physiologically relevant settings. Our results show that the RNAP clamp can populate additional long-lived clamp conformational states and can switch between these states and the previously observed short-lived clamp states. Our results further show that the RNAP clamp exhibits unchanged conformational dynamics in the presence of elevated  $K^+$ , and decreased conformational dynamics in the presence of elevated  $Mg^{2+}$ ; exhibits enhanced conformational dynamics in the presence of molecular crowding; and show that most RNAP molecules engaged in nonspecific interaction with DNA exhibit a closed clamp conformation. Taken together, the results show that clamp conformation and dynamics vary under different solution conditions and offer insight into how modulation of clamp motions might impact transcription regulation.

## MATERIALS AND METHODS

### RNAP preparation

Fluorescently labelled, hexahistidine-tagged *Escherichia coli* RNAP holoenzyme (hereafter ‘clamp labelled RNAP’)

with Cy3B and Alexa647 at positions 284 on the  $\beta'$  subunit, and 106 on the  $\beta$  subunit, respectively, were prepared using an *in vivo* reconstitution as described in (16).

### DNA

Oligonucleotides were purchased from Sigma Aldrich and annealed in hybridization buffer (10 mM Tris–HCl pH 8.0, 50 mM NaCl, 1 mM EDTA). The sequence for the non-specific DNA was generated from the lacCONS promoter sequence (15) by full substitution of the –35 and –10 elements (in purple), as follows:

```
5'-AGGCGCTGTCCTTTATGCTTCGGCTCGCCGGT
  AGTGTGGAATTGTGAGAGCGGATAACAATTC-
  3'
3'-TCCGCGACAGGAAATACGAAGCCGAGCGGC
  CATCACACCTTAACACTCTCGCCTATTGTTAA
  AG-5'
```

### Formation of RNAP complexes with non-promoter DNA

RNAP complex with non-specific DNA were prepared by mixing 20 nM of biotinylated-non-specific dsDNA with 50 nM labelled RNAP for 5 min at 37°C in KG7 buffer (40 mM HEPES–NaOH, pH 7.0, 100 mM potassium glutamate, 10 mM  $MgCl_2$ , 1 mM dithiothreitol and 5% glycerol).

### Single-molecule fluorescence imaging of RNAP under different conditions

For all single-molecule experiments except experiments in Figure 3B, a biotin-PEG-passivated glass surface was prepared, functionalized with neutravidin and treated with biotinylated anti-hexahistidine monoclonal antibody (Qiagen) as described (15). RNAP immobilization was performed by adding 100 pM solution of labelled RNAP holoenzyme to the PEGylated surfaces with biotinylated anti-hexahistidine monoclonal antibody (15) for 5 min at 22°C in KG7 buffer (40 mM HEPES–NaOH, pH 7.0, 100 mM potassium glutamate, 10 mM  $MgCl_2$ , 1 mM dithiothreitol, 5% glycerol). Observation wells containing immobilized labelled RNAP were washed with  $3 \times 50 \mu\text{l}$  KG7. For experiments performed under different solution conditions the following solution mixtures were added to the observation wells 3 min before recording of the movie. For experiments in Figure 1: 30  $\mu\text{l}$  KG7 imaging buffer (40 mM HEPES–NaOH, pH 7.0, 100 mM potassium glutamate, 10 mM  $MgCl_2$ , 1 mM dithiothreitol, 5% glycerol and 2 mM TROLOX, plus an oxygen scavenging system consisting of 1 mg/ml glucose oxidase, 40  $\mu\text{g}/\text{ml}$  catalase and 1.4% w/v D-glucose).

For experiments in Figure 3A: 30  $\mu\text{l}$  KG7 imaging buffer supplemented with 20% PEG-8000. For experiments in Figure 2A: 30  $\mu\text{l}$  imaging buffer with 1M KCl (40 mM HEPES–NaOH, pH 7.0, 1000 mM potassium chloride, 10 mM  $MgCl_2$ , 1 mM dithiothreitol, 5% glycerol and 2 mM TROLOX, plus an oxygen scavenging system consisting of 1 mg/ml glucose oxidase, 40  $\mu\text{g}/\text{ml}$  catalase and 1.4% w/v D-glucose).

For experiments in Figure 2B: 30  $\mu\text{l}$  imaging buffer with no  $\text{Mg}^{2+}$  or 25 mM  $\text{Mg}^{2+}$  or 100 mM  $\text{Mg}^{2+}$  (40 mM HEPES–NaOH, pH 7.0, 1 M potassium chloride, 0 or 25 mM or 100 mM  $\text{MgCl}_2$ , 1 mM dithiothreitol, 5% glycerol and 2 mM TROLOX, plus an oxygen scavenging system consisting of 1 mg/ml glucose oxidase, 40  $\mu\text{g/ml}$  catalase, and 1.4% w/v D-glucose). For experiments in Figure 3B, 100 pM RNAP-non-specific DNA complex was added to a biotin-PEG-passivated glass surface functionalized with neutravidin and incubated for 5 min at 22°C in KG7 buffer. Observation wells containing immobilized labelled RNAP were washed with  $3 \times 50 \mu\text{l}$  KG7 and 30  $\mu\text{l}$  KG7 imaging buffer (40 mM HEPES–NaOH, pH 7.0, 100 mM potassium glutamate, 10 mM  $\text{MgCl}_2$ , 1 mM dithiothreitol and 5% glycerol, 2 mM TROLOX, plus an oxygen scavenging system consisting of 1 mg/ml glucose oxidase, 40  $\mu\text{g/ml}$  catalase, 1.4% w/v D-glucose) was added just before movies were recorded.

### Single-molecule fluorescence instrumentation

Single-molecule FRET experiments were performed on a custom built objective-type total-internal-reflection fluorescence (TIRF) microscope (17). Light from a green laser (532 nm; Samba; Cobolt) and a red laser (635 nm; CUBE 635-30E, Coherent) was combined using a dichroic mirror, coupled into a fiber-optic cable, focused onto the rear focal plane of a 100 $\times$  oil-immersion objective (numerical aperture 1.4; Olympus), and displaced off the optical axis such that the incident angle at the oil-glass interface exceeds the critical angle, creating an evanescent wave. Alternating-laser excitation (ALEX) was implemented by directly modulating the two lasers using an acousto-optical modulator (1205C, Isomet). Fluorescence emission was collected from the objective, separated from excitation light by a dichroic mirror (545 nm/650 nm, Semrock) and emission filters (545 nm LP, Chroma; and 633/25 nm notch filter, Semrock), focused on a slit to crop the image, and then spectrally separated (using a dichroic mirror; 630 nm DLRP, Omega) into donor and emission channels focused side-by-side onto an electron-multiplying charge-coupled device camera (EMCCD; iXon 897; Andor Technology). A motorized x/y-scanning stage with continuous reflective-interface feedback focus (MS-2000; ASI) was used to control the sample position relative to the objective.

### Image analysis and data processing

Movies of surface-immobilized labeled RNAP were analysed using the home-built software TwoTone (17), and the background-corrected intensity-vs.-time traces for donor emission intensity upon donor excitation ( $I_{DD}$ ), acceptor emission intensity upon donor excitation ( $I_{DA}$ ), and acceptor emission intensity upon acceptor excitation ( $I_{AA}$ ) were extracted as described (17). For each dataset, we manually inspected intensity time traces and exclude traces exhibiting multiple-step donor or acceptor photobleaching; traces exhibiting donor or acceptor photobleaching in frames 1–50; and traces exhibiting donor or acceptor blinking. The set of selected intensity time traces were used to calculate time traces of apparent donor–acceptor FRET efficiency ( $E^*$ )

and donor–acceptor stoichiometry ( $S$ ), as described (18):

$$E^* = I_{DA} / (I_{DD} + I_{DA})$$

$$S = (I_{DA} + I_{DD}) / (I_{DD} + I_{DA} + I_{AA})$$

The  $E^*$  time traces include only data points preceding any donor or acceptor photobleaching events. Two-dimensional  $E^*$ – $S$  plots were constructed using all selected data points to distinguish species containing donor only (D-only), acceptor only (A-only), and both donor and acceptor (D–A). For species containing both donor and acceptor (D–A), 1D  $E^*$  histograms were plotted.

### HMM analysis of FRET time-traces

The set of  $E^*$  time traces selected for analysis were analysed using Hidden Markov Modelling as implemented in the ebFRET software (19); and fitted to models with two to six distinct  $E^*$  states. The models were evaluated based on estimated values for lower bound per series ( $L$ ). A higher value of  $L$  indicates a better fit of model to data (19). In order to avoid overfitting, we determined the increase in  $L$  ( $\Delta L$ ) as the number of  $E^*$ -states were raised by one, starting from a model of 2-states, and chose a model after which no significant increase in  $L$  (i.e.  $\Delta L < 1.0$ ) was observed. For all experiments except two in Figure 2B (datasets corresponding to 25 mM or 100 mM  $\text{Mg}^{2+}$ ) we estimated that a three-state model best describes our data and for experiments in Figure 2B, a two-state model provides the best description. The apparent FRET efficiencies ( $E^*$ ) from the fit to a two- or three-state model were extracted, plotted in Origin (Origin Lab) for the overall population, as well as for the static subpopulation alone, and the dynamic subpopulation alone. The resulting  $E^*$  histograms linked to each state were fitted to single Gaussian functions in Origin. The resulting histograms provide the equilibrium population distributions of states with distinct  $E^*$ , define percentages of subpopulations with distinct  $E^*$  ( $P$ ), and, for each subpopulation, define mean  $E^*$ . The errors in mean  $E^*$  and  $P$  were estimated from parameters obtained from Gaussian fitting to the data in Origin. For transition-rate measurements, an HMM analysis was applied to time-traces exhibiting dynamic behaviour. To identify dynamic traces from the set of selected molecules, individual traces were manually checked and those showing anti-correlated changes in the DD and DA channel were identified. Molecules showing greater than three transitions were assigned as dynamic. The dataset comprising dynamic molecules were fitted to a two- or three-state model, and rates of transitions between the states,  $k_{ij}$  (where  $i$  and  $j$  are the states before and after transition), were calculated by multiplying the transition probabilities per frame with the number of frames per second. Average transition rates between states and corresponding errors were calculated for each experiment from three separate groups of molecules. Mean lifetime in a clamp conformational state,  $i$ , was estimated from the transition rates out of that state as  $1/(\sum k_{ij})$ .

### Simulation of FRET traces

We used Hidden Markov Models for our three-state system simulation. The transition probability matrix of the



three-state model was calculated from the rates obtained in the short-frame time experiments (20-ms per frame). To check the validity of our approach we first performed simulations using this transition probability matrix to generate time traces with the short-frame time of 20-ms. To estimate a Gaussian noise in FRET efficiency, we measured the standard deviations of FRET efficiency in static traces from experiments performed at 20-ms frame time. The mean of these, 0.070, was then applied to all simulated FRET time traces as the standard deviation of Gaussian noise. We generated 200 simulated traces with 470 frames (Supplementary Figure S2A, *left*). These numbers were selected as it represents typical numbers from the experimental data. HMM analysis on the simulated traces were performed using ebFRET as described previously, to determine mean  $E^*$  for each state and transition rates between the states. HMM-derived histograms from the simulated dataset showed  $E^*$  distributions centred around  $\sim 0.20$  (32%),  $\sim 0.30$  (52%) and  $\sim 0.42$  (16%) (Supplementary Figure S2B, *left*); rates for clamp opening motions,  $k_{C-PC}$ ,  $k_{PC-O}$ , and  $k_{C-O}$ , of  $\sim 4.3$ , 1.0 and  $0.2 \text{ s}^{-1}$ ; and rates of clamp-closing motions,  $k_{PC-C}$ ,  $k_{O-PC}$  and  $k_{O-C}$ , of  $\sim 1.4$ , 1.5 and  $0.2 \text{ s}^{-1}$ , respectively (Supplementary Figure S2B, *left*; S2C). These results were in excellent agreement with the results for the sub-population of dynamic molecules corresponding to the shorter-span (20-ms) experiments (Supplementary Figure S1A and Table 1, Supplementary Table S1 for experimental results and Supplementary Figure S2 for simulations). Next, to simulate FRET time traces under long-frame time (200-ms) conditions, using rates obtained in the short-frame time experiments, we binned the 20-ms time traces into 200-ms time traces by averaging 10 frames. We estimated a value of 0.068 as the standard deviation of Gaussian noise using the procedure described above and simulated 200 traces with 600 frames. The simulated traces were split into three subgroups and HMM analysis was performed on them (as described for the experimental datasets) to extract average transition rates and corresponding errors (s.d.). All simulations were implemented in MATLAB.

## RESULTS

### Detection of RNAP clamp conformation and conformational dynamics

Consistent with previous smFRET studies on RNAP clamp conformation and conformational dynamics (13,15,16), the current experiments with surface-immobilized, doubly labelled RNAP derivatives having fluorophores incorporated at the tip of the RNAP clamp and the tip of the opposite wall of the RNAP active-site cleft (clamp labelled RNAP; Figure 1A, B) showed that, in RNAP holoenzyme, the RNAP clamp populates three conformational states: (i) open (mean  $E^* \sim 0.20$ ; 39%), (ii) partly closed (mean  $E^* \sim 0.30$ ; 40%) and (iii) closed (mean  $E^* \sim 0.42$ ; 21%) clamp states (Figure 1C, *left*; Supplementary Table S1). Also consistent with previous smFRET studies on RNAP clamp conformation and conformational dynamics (15,16), 30% of the molecules exhibited a ‘dynamic’ clamp conformational status (i.e. exhibited transitions between the three conformational states; Figure 1C, *right*), and  $\sim 70\%$

of molecules showed ‘static’ behaviour (i.e. did not exhibit detectable transitions between the three conformational states with our observation time of  $\sim 10 \text{ s}$  and our observation-time resolution of 20 ms; Figure 1C, *middle*). HMM-analysis of ‘dynamic’ molecules revealed that the RNAP clamp populates short-lived states corresponding to open (mean  $E^* \sim 0.22$ ; 29%), partly closed (mean  $E^* \sim 0.31$ ; 49%), and closed (mean  $E^* \sim 0.43$ ; 22%) clamp states (Supplementary Figure S1A, *left*). An estimation of transition rates from these molecules showed that the rates for the three possible clamp-opening transitions, closed clamp to partly closed clamp ( $k_{C-PC}$ ), partly closed clamp to open clamp ( $k_{PC-O}$ ) and closed clamp to open clamp ( $k_{C-O}$ ) were  $\sim 4.3$ , 0.9 and  $0.3 \text{ s}^{-1}$ , respectively, and showed that the rates of the three possible clamp-closing transitions, partly closed clamp to closed clamp ( $k_{PC-C}$ ), open clamp to partly closed clamp ( $k_{O-PC}$ ) and open clamp to closed clamp ( $k_{O-C}$ ) were  $\sim 1.4$ , 1.6 and  $0.1 \text{ s}^{-1}$ , respectively (Supplementary Figure S1B, *left*; Table 1). Further we estimated average time spent in the open, partly closed and closed clamp states to be  $\sim 0.6$ ,  $\sim 0.5$  and  $\sim 0.2 \text{ s}$ , respectively (Table 1).

### The RNAP clamp populates long-lived dynamic conformational states

Previous work showed that the RNAP clamp adopts exclusively a closed conformation upon formation of RPo (13,15), implying that that all molecules of RNAP holoenzyme that exhibit ‘static’ open and partly closed conformations are able to adopt a closed conformation upon addition of promoter DNA and formation of RPo (13,15). The existence of RNAP molecules that do not show detectable transitions between different clamp states in RNAP holoenzyme, but that, nevertheless, are able to undergo transitions to a closed-clamp conformational state upon formation of RPo, raises the possibility that, in RNAP holoenzyme, the RNAP clamp may populate not only the three characterized sub-second-timescale dynamic conformational states, but also longer-lived dynamic conformational states for which conformational transitions to other states occur on time scales substantially longer than the  $\sim 10 \text{ s}$  observation span of the experiments in Figure 1A and in previous work (15).

To assess this possibility, we extended the mean observation span from  $\sim 10$  to  $\sim 120 \text{ s}$ . To do this, we increased the frame time from 20 to 200 ms, and, to mitigate increased photobleaching with increased observation time, we decreased the laser power by  $\sim 20$ -fold and observed an increase in observation span from  $\sim 10$  to  $\sim 120 \text{ s}$ . We observed that increasing the observation-span from  $\sim 10$  to  $\sim 120 \text{ s}$  increased the fraction of molecules of RNAP holoenzyme that show dynamics from  $\sim 30\%$  to  $\sim 75\%$  (Figure 1C versus Figure 1D, *right*), with only few molecules (25%) showing no dynamic behaviour even during the extended observation span (Figure 1D, *middle*). HMM analysis of time-trajectories for this dataset showed mean  $E^*$  values for open, partly closed and closed clamp states at 0.19, 0.29 and 0.48, respectively (Figure 1D, *left*; Supplementary Table S1). We note that the mean  $E^*$  for the closed clamp conformation for the longer-span experiments appears at a higher  $E^*$  value compared to that for the previous shorter-span experiments ( $E^* \sim 0.48$  for longer-span experiments versus

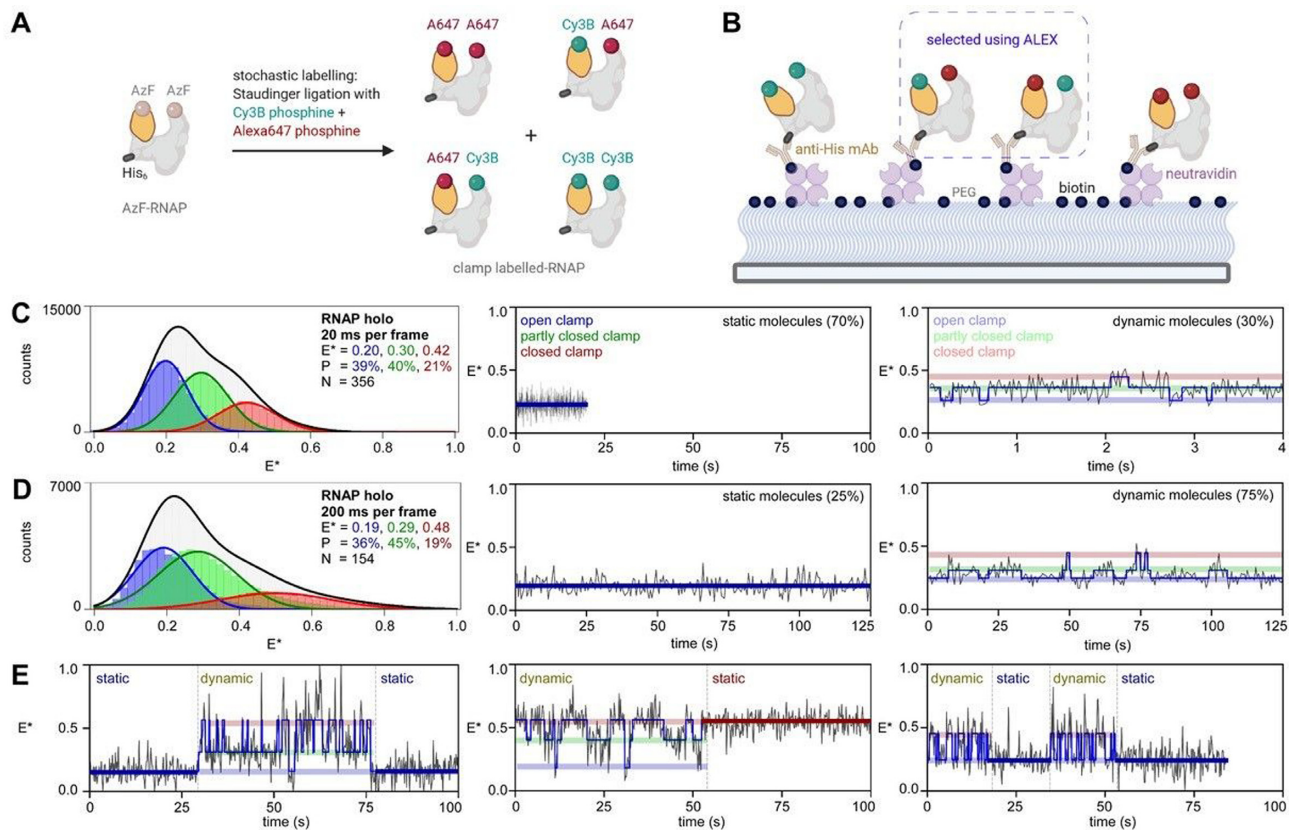


**Figure 1.** RNAP clamp switches between long-lived and short-lived conformational sub-states. (A) Stochastic labeling strategy used for generating clamp-labeled RNAP. Positions of donor (Cy3B), acceptor (Alexa647) and  $\beta'$  C-terminal hexahistidine tag are shown; Grey, RNAP; Yellow, clamp. (B) Schematic showing experimental strategy for smFRET on surface immobilized clamp-labeled RNAP. (C) (*left*) Histograms and Gaussian fits of HMM-derived  $E^*$  distributions from experiments with 20-ms frame rate for all molecules, showing open (blue), partly closed (green) and closed (red) clamp states; P, subpopulation percentage. N, number of molecules; black line, sum of gaussian fits to the three states; (*middle*) representative time traces of FRET efficiency,  $E^*$ , showing a molecule in a static open clamp state. (*right*) representative time trace of  $E^*$ , for a dynamic molecule showing hidden-Markov-model (HMM)-assigned states and inter-state transitions (blue line). Laser powers were 3.5 mW in green and 0.75 mW in red. (D) (*left*) Histograms and Gaussian fits of HMM-derived  $E^*$  distributions from experiments with 200-ms frame rate for all molecules; Colors and symbols as in C; (*middle*) representative time trace of  $E^*$ , showing a molecule in a static open clamp state. (*right*) representative time trace of FRET efficiency,  $E^*$ , for a dynamic molecule showing HMM-assigned states. Laser powers were 0.20 mW in green and 0.075 mW in red. (E) (*left*) Time trace of  $E^*$ , showing transition between a static open clamp status to a dynamic status (*middle*) time trace of  $E^*$ , showing transition between a dynamic status to a static closed clamp status (*right*) time trace of  $E^*$ , showing transitions between dynamic and static clamp status. Laser powers and frame rate as in D.

$E^* \sim 0.42$  for 20-ms frame rate experiments; Supplementary Table S1). One possible origin of this difference may be that for 20-ms exposure experiments although we can resolve three conformational states, the closed-clamp state contain unresolved and kinetically distinct conformations. It is possible one or more of these unresolved closed clamp conformations had a very short lifetime such that they can be captured in the 20-ms exposure experiments but are missed in the 200-ms experiments resulting in a shift in the  $E^* \sim 0.42$  peak at 20-ms exposure to  $E^* \sim 0.48$  at 200-ms exposure.

HMM-analysis for the subpopulation of dynamic molecules revealed that the RNAP clamp populates states corresponding to open (mean  $E^* \sim 0.19$ ; 36%), partly closed (mean  $E^* \sim 0.28$ ; 43%), and closed (mean  $E^* \sim 0.50$ ; 21%) clamp states (Supplementary Figure S1A, *right*). Estimated transition rates from these ‘dynamic’ molecules indicated that rates for clamp-opening motions,  $k_{C-PC}$ ,  $k_{PC-O}$  and  $k_{C-O}$  were  $\sim 0.5$ , 0.2 and 0.02  $s^{-1}$ , respectively, and that rates of clamp-closing motions,  $k_{PC-C}$ ,  $k_{O-PC}$  and  $k_{O-C}$  were  $\sim 0.3$ , 0.3 and 0.02  $s^{-1}$ , respectively

(Supplementary Figure S1B, *right*; Table 1). The observed transition rates were  $\sim 4$ –10-fold slower as compared to those observed in the previous, shorter-span experiments (Table 1). The longer-span experiments also showed much longer average dwells in individual clamp conformational states of  $\sim 3.2$ , 2.1 and 2.0 s corresponding to open clamp, partly closed clamp and closed clamp conformations, respectively as compared to the previous shorter-span experiments (Table 1).

An inspection of individual FRET time-trajectories showed molecules ( $\sim 14\%$ ) that populate a very long-lived clamp conformational state (stable for  $> 20$  s) before switching to another clamp conformation (Figure 1E, *left*) as well as molecules that exhibit a ‘dynamic’ clamp status (rapid switching between relatively short-lived clamp conformational states) but transition to a very long-lived clamp conformational state at a later time-point (Figure 1E, *middle*). Further, among these molecules, a few ( $\sim 2\%$ ), show repeated switching between short-lived clamp conformational states and a very long-lived clamp conformational state

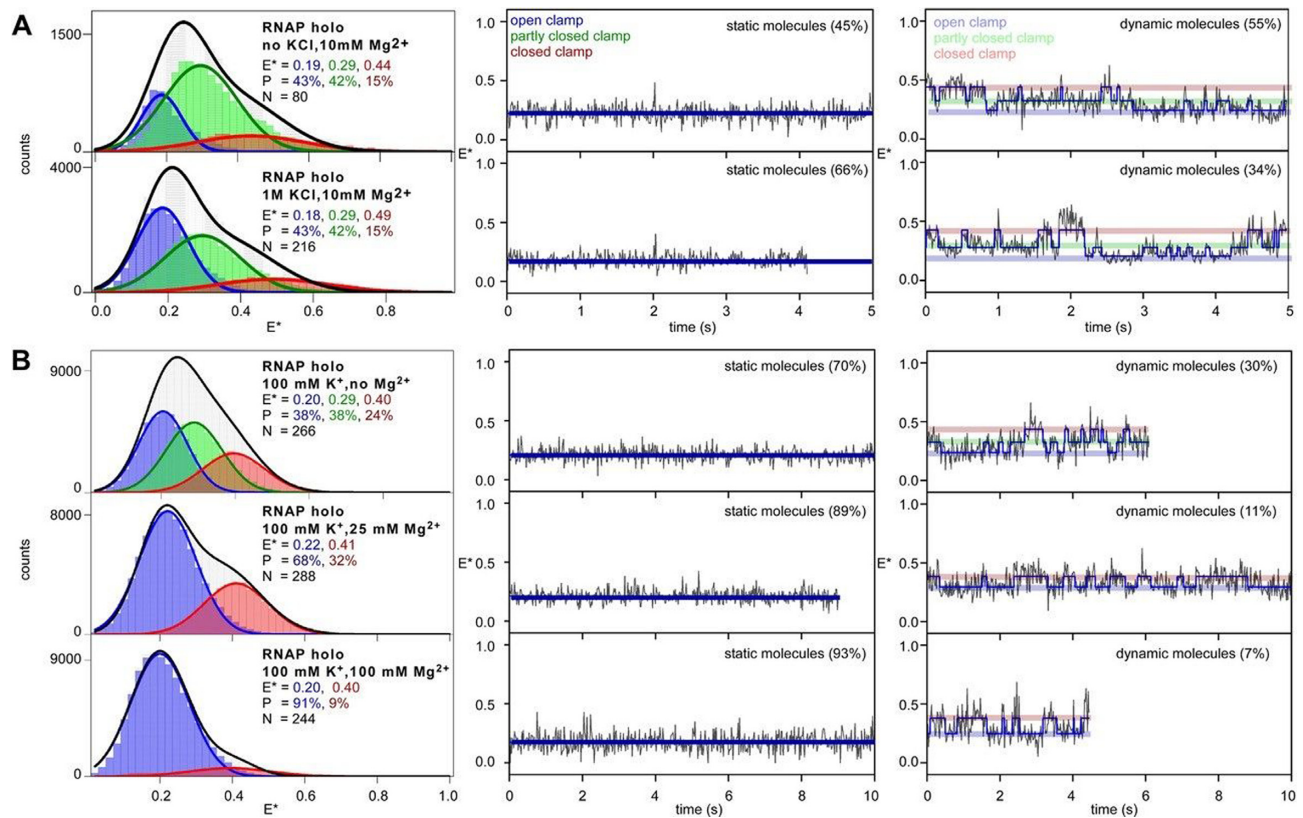


**Figure 2.** Modulation of RNAP clamp conformation by different concentrations of a monovalent and a divalent salt. **(A)** smFRET data monitoring clamp conformation in presence of no K<sup>+</sup> (*top*) or 1000 mM K<sup>+</sup> concentration (*bottom*). (*left subpanels*) histograms and Gaussian fits of HMM-derived  $E^*$  distributions for all molecules, showing open (blue), partly closed (green) and closed (red) clamp states; P, subpopulation percentage; N, number of molecules; black line, sum of gaussian fits to the three states; (*middle subpanels*) representative time trace of  $E^*$ , showing a molecule in a static open clamp state (*right subpanels*) representative time trace of  $E^*$ , for a dynamic molecule showing HMM-assigned states, and interstate transitions (blue line). **(B)** smFRET data monitoring clamp conformation in presence of increasing Mg<sup>2+</sup> concentrations (no Mg<sup>2+</sup>, 25 mM Mg<sup>2+</sup> and 100 mM Mg<sup>2+</sup>). (*left subpanels*) histograms and Gaussian fits of HMM-derived  $E^*$  distributions for all molecules; Colors and symbols as in A; (*middle subpanels*) representative time traces of  $E^*$ , showing molecules in a static open clamp state (*right subpanels*) representative time trace of  $E^*$ , for a dynamic molecule showing hidden-Markov-model (HMM)-assigned states and interstate transitions (blue line). Relative percentages of the populations are inset. Frame rate was 20 ms and laser powers were 3.5 mW in green and 0.75 mW in red.

(Figure 1E, *right*). The observed interconversions between very long-lived and short-lived conformational states, and the overall decreased rates for transitions among different clamp conformations, may be a result of two possible scenarios. In the first scenario, we may be missing transitions between clamp conformations as a result of slower frame rate of the experiment, i.e. entire dwells corresponding to different clamp conformational states are being missed, as the dwell times in these states are shorter than the time of individual frames (i.e. dwells shorter than 200 ms), resulting in artificially long dwells in a clamp conformational state and lead to an overall lowering of observed transition rates. From the transition rates measured from the 20-ms frame experiments, we estimate that ~30%, 41% and 57% dwells in the open, partly closed and closed clamp states would be missed in experiments with 200-ms frames. In the second scenario, there may be transitions between kinetically different clamp conformational states with similar FRET values resulting in longer dwells. As an example, transitions between a long-lived open clamp state and a short-lived open

clamp state would result in an artificially longer dwell in the open-clamp state where all transitions between these two states are missed as they have identical FRET values. It is possible that such artificially long dwells are mostly missed in experiments conducted at ~20-ms exposure (shorter observation span of ~10 s), while we are able to capture a significant proportion of them in experiments conducted at ~200-ms exposure (longer observation span of ~120 s).

To understand the origin of this behaviour, we simulated FRET time trajectories at a frame rate of 200-ms per frame using transition rates obtained from the 20-ms frame time experiments in Figure 1C. The set of simulated FRET time-trajectories were analysed in a similar manner as for the experimentally obtained dataset. Analysis of the simulated dataset (200-ms per frame) showed rates of clamp opening motions,  $k_{C-PC}$ ,  $k_{PC-O}$  and  $k_{C-O}$  to be ~1.3, 0.6 and 0.3 s<sup>-1</sup>, respectively, and, rates of clamp closing motions,  $k_{PC-C}$ ,  $k_{O-PC}$  and  $k_{O-C}$  to be ~0.7, 1.2 and 0.2 s<sup>-1</sup>, respectively (Supplementary Figure S2C). We observed three main differences between the simulated dataset and experimental dataset (both with frame rate of 200-ms):



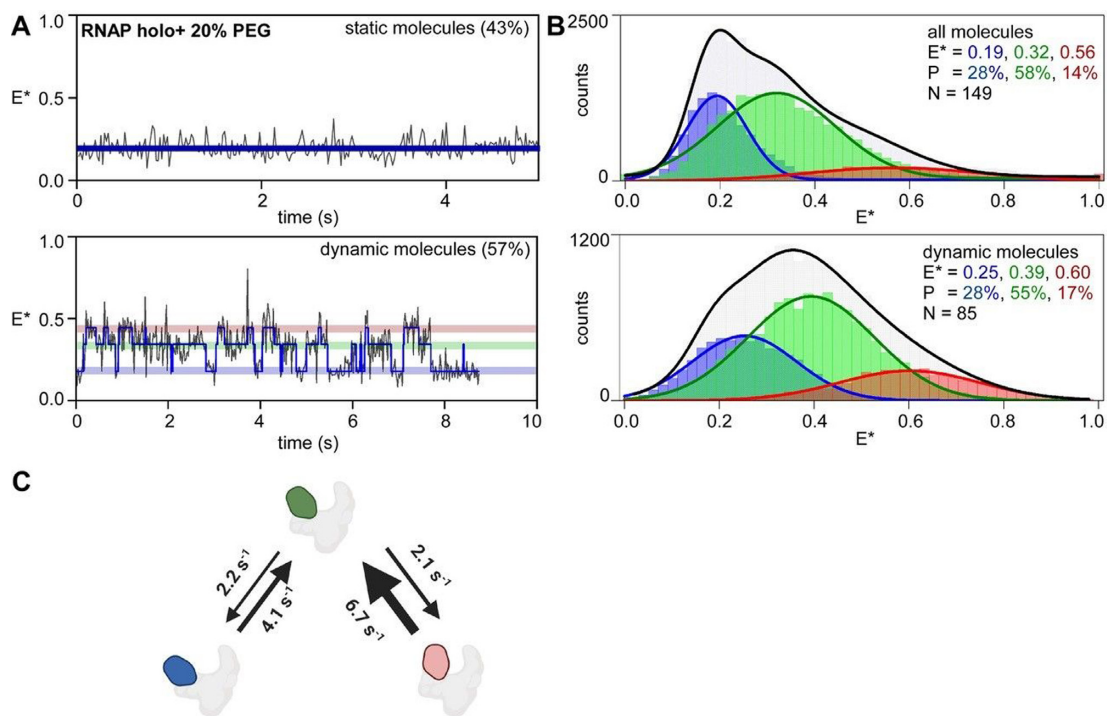


**Figure 3.** RNAP clamp exhibit enhanced dynamics under conditions of macromolecular crowding. (A) smFRET data monitoring clamp conformation in presence of 20% polyethylene glycol (PEG). (top left) representative time trace of  $E^*$ , showing a molecule in a static open clamp state (bottom left) representative time trace of  $E^*$ , for a dynamic molecule showing HMM-assigned states, and interstate transitions (blue line). (B) Histograms and Gaussian fits HMM-derived  $E^*$  distributions for all molecules (top) or only dynamic molecules (bottom), showing open (blue), partly closed (green) and closed (red) clamp states;  $P$ , subpopulation percentage;  $N$ , number of molecules; black line, sum of gaussian fits to the three states. (C) Transition rates between clamp conformational states. Blue, open clamp; green, partly closed clamp; red, closed clamp; grey, rest of RNAP. Frame rate was 20 ms and laser powers were 3.5 mW in green and 0.75 mW in red.

**Table 1.** Transition rates and dwell times for clamp conformations under different conditions

	$K^+$ (mM)	$Mg^{2+}$ (mM)	$\tau$ (ms)	Transition rates ( $s^{-1}$ )						Dwell times (s)		
				$k_{O-PC}$	$k_{O-C}$	$k_{PC-O}$	$k_{PC-C}$	$k_{C-O}$	$k_{C-PC}$	$t_O$	$t_{PC}$	$t_C$
RNAP	100	10	20	$1.55 \pm 0.21$	$0.14 \pm 0.03$	$0.87 \pm 0.16$	$1.36 \pm 0.54$	$0.26 \pm 0.08$	$4.32 \pm 0.42$	$0.59 \pm 0.07$	$0.45 \pm 0.11$	$0.22 \pm 0.02$
RNAP	100	10	200	$0.29 \pm 0.03$	$0.02 \pm 0.01$	$0.23 \pm 0.01$	$0.25 \pm 0.05$	$0.02 \pm 0.01$	$0.49 \pm 0.24$	$3.20 \pm 0.30$	$2.10 \pm 0.20$	$2.00 \pm 0.20$
RNAP	100	0	20	$1.67 \pm 0.09$	$0.18 \pm 0.13$	$0.48 \pm 0.14$	$1.67 \pm 0.14$	$0.07 \pm 0.02$	$5.14 \pm 1.42$	$0.54 \pm 0.05$	$0.47 \pm 0.04$	$0.19 \pm 0.05$
RNAP	1000	10	20	$1.92 \pm 0.38$	-	$1.00 \pm 0.06$	$2.21 \pm 0.35$	-	$6.17 \pm 1.53$	$0.50 \pm 0.10$	$0.31 \pm 0.03$	$0.16 \pm 0.04$
RNAP	0	10	20	$3.48 \pm 0.39$	-	$1.66 \pm 0.24$	$1.44 \pm 0.07$	-	$3.55 \pm 0.11$	$0.29 \pm 0.03$	$0.33 \pm 0.03$	$0.28 \pm 0.01$
RNAP+non-specific DNA	100	10	100	$0.34 \pm 0.06$	-	$0.10 \pm 0.02$	$0.25 \pm 0.01$	-	$0.54 \pm 0.04$	$2.60 \pm 0.40$	$2.90 \pm 0.20$	$1.80 \pm 0.10$
RNAP+20% PEG-8000	100	10	20	$4.11 \pm 0.73$	-	$2.15 \pm 0.25$	$2.11 \pm 0.03$	-	$6.70 \pm 0.56$	$0.24 \pm 0.04$	$0.24 \pm 0.01$	$0.15 \pm 0.01$

- (a) The transition rates for the experimental dataset are lower than that obtained from the simulated dataset by  $\sim 2$ –5 fold (Table 1).
- (b) A visual inspection of the FRET time trajectories in the simulated dataset (Supplementary Figure S2A, right) did not reveal any time trajectories like those on the experimental dataset (Figure 1E), which show very long-lived clamp conformational states (stable for  $>20$  s).
- (c) FRET histograms obtained from the simulated dataset differ from that obtained for the dynamic molecules in the experimental dataset, with  $\sim 27\%$ ,  $54\%$  and  $19\%$  (Supplementary Figure S2B, right) of the time spent in the open, partly closed and closed clamp state, respectively, in the simulated dataset as compared to  $\sim 36\%$ ,  $43\%$  and  $21\%$  (Supplementary Figure S1B) of the time spent in the open, partly closed and closed clamp state, respectively, in the experimental dataset.

Since the simulations were performed at a frame rate of 200-ms using transition rates from the experimental dataset recorded at a frame rate of 20-ms, the simulated dataset should be able to recapitulate all features which result from missed dwells. A large difference between experimental and simulated dataset, as noted above, indicate that the result of experiments performed at a frame rate of 200 ms cannot be explained solely as an effect of missed dwells. These results strongly suggest that extension of the observation span enables us to capture dwells with hidden transitions between long-lived and short-lived clamp conformational states which are structurally similar in terms of the clamp conformation (i.e. having similar FRET values), and this is reflected in the time trajectories which show very long-lived clamp conformational states (Figure 1E). Additionally, we note that, from an analysis of the simulated dataset, that in the absence of any hidden transitions, the average dwell times in the respective clamp conformational states

for 200-ms frame experiments should be  $\sim 0.8$ ,  $0.8$  and  $0.6$  s for open, partly closed and closed clamp states (Supplementary Figure S2C). A careful look at the dwells corresponding to the different clamp conformational states obtained from simulations performed at a frame rate of 200-ms show that the number of really long dwells ( $>5.0$  s) corresponding to open clamp ( $\sim 0.5\%$ ), partly closed clamp ( $\sim 5\%$ ) and closed clamp ( $\sim 0.1\%$ ) conformational states were only few in number. In contrast, the experimentally obtained mean dwell times for each state were much longer, for open clamp ( $\sim 3.2$  s), partly closed clamp ( $\sim 2.1$  s) and closed clamp ( $\sim 2.0$  s) conformational states (Table 1), and the relative number of really long dwells ( $>5.0$  s) were significantly more for open clamp ( $\sim 29\%$ ), partly closed clamp ( $\sim 19\%$ ) and closed clamp ( $\sim 11\%$ ) states. We suggest therefore that these very long dwells in the experimental datasets correspond to either long-lived clamp conformational states or compound dwells consisting of both long-lived and short-lived states with one or more hidden transitions between them.

### The RNAP clamp exhibits unchanged clamp dynamics in the presence of elevated concentrations of a monovalent-cation

For all our previous experiments on clamp conformational dynamics, we used buffers with 100 mM monovalent ( $\text{K}^+$ ) and 10 mM divalent ( $\text{Mg}^{2+}$ ) salt concentrations. To check if salt with either monovalent or divalent cations influence the clamp status or dynamics, we used different concentrations of each of  $\text{K}^+$  and  $\text{Mg}^{2+}$  to monitor clamp dynamics, in separate experiments performed as described previously at a frame rate of 20 ms. First, we performed experiments in absence of any  $\text{K}^+$ , and observed  $\sim 22\%$  of open clamp ( $E^* \sim 0.19$ ),  $\sim 61\%$  of partly closed clamp ( $E^* \sim 0.29$ ) and  $17\%$  of closed clamp ( $E^* \sim 0.44$ ) conformations (Figure 2A, top; Supplementary Table S1), with 68% ‘static’ molecules (Figure 2A, top middle) and 32% ‘dynamic’ molecules (Figure 2A, top right). Further analysis for the subpopulation of dynamic molecules showed that the clamp populates states corresponding to open (mean  $E^* \sim 0.19$ ; 24%), partly closed (mean  $E^* \sim 0.31$ ; 45%), and closed (mean  $E^* \sim 0.44$ ; 31%) clamp states (Supplementary Figure S3A, top). From HMM-analysis of dynamic molecules we observed similar transition rates between closed clamp and partly closed clamp conformations ( $k_{\text{C-PC}}$  and  $k_{\text{PC-C}}$  of  $\sim 3.6$  and  $\sim 1.4$   $\text{s}^{-1}$ ; Table 1) and modestly enhanced transition rates between open and partly closed clamp ( $k_{\text{PC-O}}$  and  $k_{\text{O-PC}}$  of  $\sim 1.7$  and  $\sim 3.5$   $\text{s}^{-1}$ ; Table 1), respectively. Direct transitions between the open and closed-clamp conformations were rare under these conditions and rates corresponding to these transitions could not be reliably estimated (Table 1). In a next experiment, we tested the effect of increased concentration of  $\text{K}^+$  (1000 mM) on the status of clamp conformation. Our results showed a similar distribution of clamp states as compared to experiments performed in presence of 100 mM  $\text{K}^+$  (Figure 2A, bottom). Specifically, we observed three clamp states: open,  $E^* \sim 0.18$  (43%); partly closed,  $E^* \sim 0.29$  (42%) and closed,  $E^* \sim 0.49$  (15%) (Figure 2A, bottom left; Supplementary Table S1), with 66% ‘static’ molecules (Figure 2A, bottom middle) and 34% ‘dynamic’ molecules (Figure 2A, bottom right). We note that although mean  $E^*$  for the open and partly-closed clamp

states were similar, the closed clamp state under these conditions exhibit a higher mean  $E^*$  as compared to that observed in presence of 100 mM  $\text{K}^+$ . Similar results were obtained for the sub-population of dynamic molecules with HMM-derived states corresponding to open, partly closed and closed clamp conformations centred around  $E^* \sim 0.20$ ,  $0.30$  and  $0.48$ , respectively (Supplementary Figure S3B). Further, estimation of transition rates from these dynamic molecules showed similar transition rates between open clamp and partly closed clamp conformations ( $k_{\text{O-PC}}$  and  $k_{\text{PC-O}}$  of  $\sim 1.9$  and  $\sim 1.0$   $\text{s}^{-1}$ ; Table 1) and modestly enhanced transition rates between closed and partly closed clamp ( $k_{\text{PC-C}}$  and  $k_{\text{C-PC}}$  of  $\sim 2.2$  and  $\sim 6.1$   $\text{s}^{-1}$ ; Table 1), respectively. Taken together we note that the overall distribution and the relative proportion of ‘static’ and ‘dynamic’ molecules for both datasets (no  $\text{K}^+$  and 1000 mM  $\text{K}^+$ ) were similar, and the estimated transition rates were only modestly different when compared to results in presence of 100 mM  $\text{K}^+$  (Figure 1A; Table 1). Therefore, we conclude that under conditions of significantly altered  $\text{K}^+$  concentrations, no drastic effect on clamp conformation and dynamics was observed.

### The RNAP clamp exhibits decreased clamp dynamics in the presence of elevated concentrations of a divalent-cation

Next, we monitored the clamp conformation in presence of increasing concentration of  $\text{Mg}^{2+}$  (no  $\text{Mg}^{2+}$ , 25 mM  $\text{Mg}^{2+}$  and 100 mM  $\text{Mg}^{2+}$ ). In presence of no  $\text{Mg}^{2+}$ , the equilibrium population distributions indicated the presence of  $\sim 38\%$  of open clamp ( $E^* \sim 0.20$ ),  $\sim 38\%$  of partly closed clamp ( $E^* \sim 0.29$ ) and  $\sim 24\%$  of closed clamp state ( $E^* \sim 0.40$ ) (Figure 2B, first row; Supplementary Table S1) with  $\sim 71\%$  molecules exhibiting a ‘static’ clamp status and  $\sim 29\%$  molecules being ‘dynamic’. HMM analysis of dynamic molecules for this dataset identified an open ( $E^* \sim 0.20$ ; 38%), partly closed ( $E^* \sim 0.29$ ; 38%) and closed ( $E^* \sim 0.40$ ; 24%) clamp states, clamp-opening rates,  $k_{\text{C-PC}}$ ,  $k_{\text{PC-O}}$  and  $k_{\text{C-O}}$  of  $\sim 5.1$ ,  $\sim 0.5$  and  $0.1$   $\text{s}^{-1}$ , and clamp-closing rates  $k_{\text{PC-C}}$ ,  $k_{\text{O-PC}}$  and  $k_{\text{O-C}}$  of  $\sim 1.7$ ,  $1.7$  and  $0.2$   $\text{s}^{-1}$ , respectively (Supplementary Figure S5). These results were similar to those obtained for clamp conformation and dynamics in presence of 10 mM  $\text{Mg}^{2+}$  (no  $\text{Mg}^{2+}$ , Figure 2B, first row, S5A; and 10 mM  $\text{Mg}^{2+}$ , Figure 1A and Table 1, Supplementary Table S1). Surprisingly, a significant change in the clamp conformation distribution was observed at 25 mM  $\text{Mg}^{2+}$ , where our dataset for all molecules fit best to a two-state model with clamp populating open ( $E^* \sim 0.22$ ; 69%) and closed ( $E^* \sim 0.41$ ; 31%) conformations (Figure 2B, left panels; Supplementary Table S1). Upon increasing the  $\text{Mg}^{2+}$  concentration to 100 mM, we observed a dramatic shift in the clamp conformation distribution to almost an exclusively open ( $E^* \sim 0.20$ ; 91%) conformation (Figure 2B, left panels; Supplementary Table S1) and a significant reduction in ‘dynamic’ molecules ( $\sim 11\%$  for 25 mM  $\text{Mg}^{2+}$ ;  $\sim 9\%$  for 100 mM  $\text{Mg}^{2+}$ ; Figure 2B, right panels), with most molecules exhibiting ‘static’ clamp status ( $\sim 89\%$  for 25 mM  $\text{Mg}^{2+}$ ;  $\sim 91\%$  for 100 mM  $\text{Mg}^{2+}$ ; Figure 2B, middle panels). The sub-population of dynamic molecules for these two datasets were too small to estimate reliable transition rates from an HMM-analysis. Overall, we conclude that elevated



concentrations of  $Mg^{2+}$  shift the conformational equilibria to a long-lived open clamp conformation.

### The RNAP clamp exhibits increased clamp dynamics in the presence of molecular crowding

In the context of a living cell, the RNAP exists in a complex mixture of other proteins, nucleic acids and small molecules. It has been estimated that the overall cellular milieu consists of  $\sim 80$ – $400$  mg/ml of other macromolecules which occupy up to  $\sim 30\%$  of volume inside the cell (20,21). Such crowded environments have been reported to exert an ‘excluded-volume’ effect resulting in a shift towards more compact conformations of the protein (22,23). Most *in-vitro* studies looking at protein behaviour in crowded environments tend to use ‘inert crowders’ like polyethylene glycol (PEG) or dextran which mimic the excluded-volume effect (22).

To examine how a crowded cellular milieu may affect RNAP clamp conformational dynamics, we used 20% polyethylene glycol (PEG-8000) in the imaging buffer to study motions of clamp at a frame rate of 20-ms. HMM analysis of time trajectories for this dataset reveals only  $\sim 43\%$  of the RNAP molecules were ‘static’ (compared to  $\sim 70\%$  molecules for the non-crowded condition; Figure 3A, *top left*), whereas most molecules showed a dynamic behaviour ( $\sim 57\%$ ; Figure 3A, *bottom left*). HMM-derived histograms for all molecules showed that, in presence of 20% PEG, the RNAP clamp populates three conformational states: open ( $E^* \sim 0.19$ ; 28%), partly closed ( $E^* \sim 0.32$ ; 58%) and closed ( $E^* \sim 0.56$ ; 14%) (Figure 3B, *top*; Supplementary Table S1). We note that the  $E^*$  distribution for the  $E^* \sim 0.56$  state, is unusually broad (width  $\sim 0.42$ ; Supplementary Table S1), and may consist of overlapping FRET states that could not be resolved under our experimental conditions. These results show an overall depopulation of the open clamp state and increase in relative abundance of the partly closed and closed clamp states compared to the non-crowded conditions (Figure 3B, *top right*; Supplementary Table S1). Additionally, we observe a shift in mean FRET efficiencies for the closed clamp conformation to higher FRET values (a shift to  $\sim 0.56$  compared to  $\sim 0.42$  for the closed clamp state; Supplementary Table S1), indicative of a much greater degree of clamp closure in these states. HMM-derived histograms for only dynamic molecules showed an even larger shift towards higher FRET values compared to those for dynamic molecules in absence of crowding (Supplementary Figure S1), with the three states now centred around  $E^* \sim 0.25$  (28%),  $E^* \sim 0.39$  (55%) and  $E^* \sim 0.60$  (17%) (Figure 3B, *bottom*; Supplementary Table S1). Taken together, these observations are consistent with expectations that macro-molecular crowding may result in stabilization of more compact protein conformations (24), and in this case, greater degree of clamp closure within RNAP molecules. Most notably, HMM-analysis of only dynamic molecules showed transition rates for clamp-opening motions,  $k_{C-PC}$  and  $k_{PC-O}$  were  $\sim 6.7$  and  $2.1$   $s^{-1}$ , respectively, and, rate of clamp closing motions,  $k_{PC-C}$  and  $k_{O-PC}$  were  $\sim 2.2$  and  $4.1$   $s^{-1}$ , respectively (Figure 3C; Table 1), under the conditions of crowding, indicating enhanced rates of switching between the different short-lived clamp conformations. Direct transitions between open and closed

conformations were rarely observed and as such it was not possible to estimate transition rates between them. Overall, the increased proportion of ‘dynamic’ molecules and the enhanced transition rates indicate an enhancement of clamp motions under conditions of macromolecular crowding.

### The RNAP clamp predominantly exhibits a closed conformation when RNAP is bound non-specifically to DNA

It has been proposed that RNAP can bind to non-specific DNA in the cell as it tries to find a promoter sequence via either 1D-sliding along genomic DNA, or via a 3D-diffusion-mediated ‘hop and search’ mechanism, or a combination of both (25–27). Further, it has been proposed that, while searching for promoters along the bacterial genome, the clamp populates an open conformation and undergoes transient clamp closures as RNAP tries to locate a promoter (5). Such proposals however, have been speculative, as no direct observation of clamp conformations or motions during promoter search has been made to date. To gain insight into RNAP clamp conformation and dynamics at non-specific DNA binding sites as would be encountered by the RNAP while searching for promoter sites, we designed a biotinylated non-specific DNA by changing the segments ( $-35$  and  $-10$  positions) of a *lac*-promoter responsible for the sequence-specific recognition by RNAP (see Materials and Methods). In a next set of experiments, we pre-formed complexes with RNAP and biotinylated non-specific DNA, immobilized pre-formed single RNAP-non-specific DNA complexes on a PEGylated glass surface via biotin on DNA, and recorded single-molecule FRET time-trajectories at frame rates of 100 ms. Since immobilization was performed via biotin on DNA, all RNAP molecules under observation were bound to non-specific DNA; in fact, control experiments showed that under our conditions, no RNAP molecules stay bound to the surface in a non-specific manner in the absence of DNA (Supplementary Figure S4). HMM analysis of the trajectories for single RNAP-non-specific-DNA complexes revealed that the clamp populates a ‘static’ conformation for the majority ( $\sim 85\%$ ) of molecules (Figure 4A, *top*) and show ‘dynamic’ behaviour for  $\sim 15\%$  of the molecules (Figure 4A, *bottom*). Relative abundances of clamp conformational states for all RNAP molecules analysed were 23%, 24% and 53% for open ( $E^* \sim 0.20$ ), partly closed ( $E^* \sim 0.33$ ) and closed clamp ( $E^* \sim 0.44$ ) conformations, respectively (Figure 4B, *top*; Supplementary Table S1). The HMM-derived  $E^*$  distribution corresponding to dynamic molecules indicated presence of open ( $E^* \sim 0.23$ ; 18%), partly-closed ( $E^* \sim 0.30$ ; 54%) and closed clamp ( $E^* \sim 0.45$ ; 28%) states for this sub-population (Figure 4B, *bottom*). Next, from the HMM-fit we estimated rates of clamp opening motions,  $k_{C-PC}$  and  $k_{PC-O}$  of  $\sim 0.5$  and  $\sim 0.3$   $s^{-1}$ , and rate of clamp closing motions,  $k_{PC-C}$  and  $k_{O-PC}$  of  $\sim 0.3$  and  $\sim 0.1$   $s^{-1}$ , respectively (Figure 4C; Table 1). Direct transitions between the open and closed clamp conformations were rare. The average observation span of these experiments was  $\sim 40$  s, and it is possible that some molecules which do not show transitions under these conditions may exhibit dynamic behaviour at a longer timescale. But overall, for observed transitions, switching rates between the clamp conformations were  $\sim 4$ –

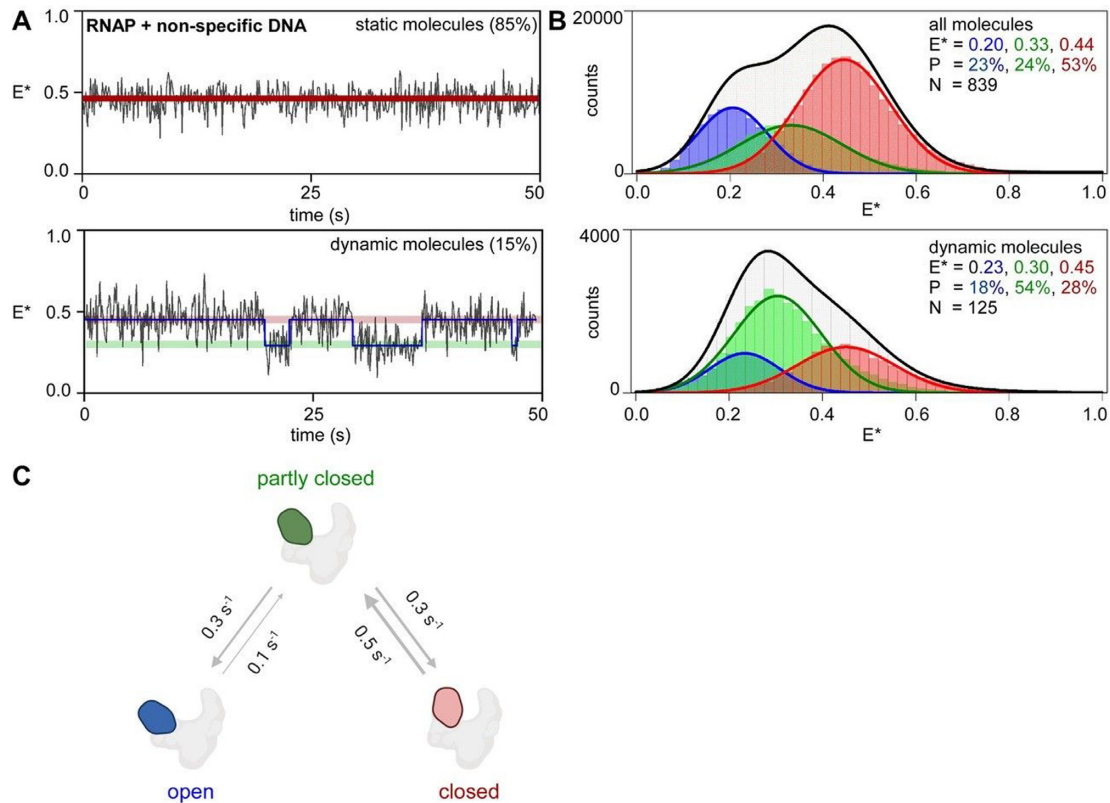


**Figure 4.** RNAP clamp mostly populates a closed clamp state when bound to non-specific DNA. (A) smFRET data monitoring clamp conformation in RNAP bound to non-specific DNA. (top left) representative time trace of  $E^*$ , showing a molecule in a static closed clamp state (bottom left) representative time trace of  $E^*$ , for a dynamic molecule showing HMM-assigned states and interstate transitions (blue line). (B) Histograms and Gaussian fits of HMM-derived  $E^*$  distributions for all molecules (top) or only dynamic molecules (bottom), showing open (blue), partly closed (green) and closed (red) clamp states;  $P$ , subpopulation percentage;  $N$ , number of molecules; black line, sum of gaussian fits to the three states. (C) Transition rates between clamp conformational states. Blue, open clamp; green, partly closed clamp; red, closed clamp; grey, rest of RNAP. Frame rate was 100 ms and laser powers were 0.50 mW in green and 0.12 mW in red.

10-fold lower and the observed dwell times were  $\sim 4$ – $10$ -fold longer, when bound to non-specific DNA, compared to those observed for free RNAP molecules under similar solution conditions (Table 1). This was in contrast with results obtained in similar experiments with preformed RNAP-promoter complexes, where the clamp was found to be in a stably closed status and did not exhibit any dynamic behaviour (13,15). We conclude that, when bound to non-specific DNA, the clamp exists in a predominantly closed conformation, but can also show very slow opening-closing dynamics.

## DISCUSSION

In this work, we build on our previous smFRET studies monitoring RNAP clamp conformation and conformational dynamics in solution (13, 15, 16) by extending the observation span of our experiments to capture structurally similar but kinetically different long-lived clamp conformations and by monitoring the clamp conformation and motions under environments RNAP molecules may encounter in a living cell, such as molecular crowding, elevated monovalent and divalent cation concentrations, and non-specific DNA binding.

Our previous smFRET studies revealed two classes of RNAP molecules depending on the nature of clamp motions: ‘static’ molecules, which show no transition to other clamp conformations, and ‘dynamic’ molecules, which show interconversion between the different clamp conformations. Here, using an extended observation span ( $\sim 120$  s), we show that previously observed molecules with a ‘static’ clamp conformation are not intrinsically different to the ‘dynamic’ molecules, but actually result from the presence of structurally similar but kinetically distinct long-lived clamp conformational sub-states, as a result of which several molecules appear to be ‘static’ at a particular clamp conformation during short observation span ( $\sim 10$  s) experiments. With the help of simulations and detailed analysis of new experiments performed at increased frame-times ( $\sim 200$  ms), we uncover the existence of long-lived clamp conformational sub-states that last for  $> 1.0$  s, a timescale at least  $\sim 3$ -fold longer than average dwell times in the short-lived conformational sub-states of  $\sim 0.3$ – $0.6$  s. Inspection of individual time-trajectories shows clear evidence of interconversion between these newly observed long-lived and previously observed short-lived clamp conformational sub-states. We note that the transition rates between these conformational sub-states potentially could result in an addi-

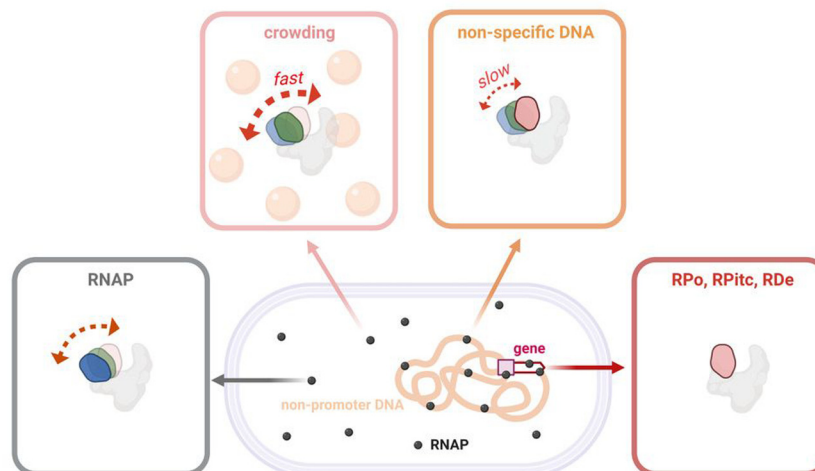


**Figure 5.** Summary of clamp conformational status in free and bound RNAP. Schematic showing clamp conformation and dynamics in free RNAP, RNAP in presence of macromolecular crowding, RNAP complexes bound to non-specific DNA, and RNAP during different stages of transcription. Black dots, RNAP; blue, open clamp; green, partly closed clamp; red, closed clamp; grey, rest of RNAP; double-headed dotted arrows, clamp motions; light orange spheres, macromolecular crowders; orange, bacterial nucleoid; rectangular purple box, promoter; white arrow, gene.

tional, previously unknown, point for modulation of clamp dynamics.

#### Modulation of clamp dynamics by altered concentrations of a monovalent and divalent salt

It is well known that both the kinetics and thermodynamics of open complex formation are heavily salt-concentration dependent (28–30). However, it is currently unknown how salt modulates conformational changes in RNAP and what role, if any, such dependence may play in the formation and stability of RPo. Interestingly, previous in-vitro measurements of thermodynamic parameters of RPo formation had found that RPo stability was drastically reduced in  $Mg^{2+}$ -containing buffers as compared to  $Na^+$ -containing buffers, with an unfavourable enthalpy component of  $\sim 18$  Kcal/mole higher in a  $Mg^{2+}$ -containing buffer (29). Since the RNA polymerase clamp is a structural element of central importance in the functioning of RNAP, here we examined how clamp dynamics are affected by changes in salt concentration. We performed experiments with altered concentrations of a monovalent salt, no  $K^+$  or very high  $K^+$  (1000 mM), and observed largely similar distributions of clamp conformations and only modestly altered transition rates between the different clamp states (Figure 2A). In contrast, intriguingly, high concentration ( $>25$  mM) of a salt with a divalent cation ( $Mg^{2+}$ ) shifts the conformational equilibria to an open clamp state, essentially abrogating any clamp-closing motions. This observation provides a simple chemical means to stabilize the open clamp conformation for further study. On the other hand, the biological relevance of the  $Mg^{2+}$  dependence is unclear, since the concentration of free  $Mg^{2+}$  inside bacterial cells is only  $\sim 1$  mM (31). However, a much large amount of cellular  $Mg^{2+}$  ( $\sim 20$ – $100$  mM) is bound to other macromolecules (ribosomes, ribozymes, nucleic acids) (31–33), and under certain cellular conditions, e.g. stress induced by antibiotics targeting ribosomes may result in higher magnesium flux in a bacterial

cell (34). Such a condition may result in a  $Mg^{2+}$ -dependent trapping of the RNAP clamp in an open conformation, resulting in down-regulation of transcription.

#### Modulation of clamp dynamics by molecular crowding

The bacterial cell also presents a crowded environment for proteins and can dramatically affect thermodynamic equilibria, diffusion properties and binding between interacting partners due to excluded-volume effects. We note that previous work on T7 RNAP had shown that the transcription initiation rates are significantly enhanced under conditions of crowding due to increase in affinity between RNAP and promoter DNA (35,36). Our results using a ‘macromolecular crowder’ (20% PEG-8000), which is expected to mimic conditions of a crowded cellular milieu (22), show a shift to a more closed conformation for the partly closed and closed clamp conformations, and an increase in the relative abundance of the partly closed state (Figure 2A) when compared with non-crowded conditions. This is consistent with the expectation that macromolecular crowding stabilises compact conformations of a protein (24). More significantly, under crowded conditions, the number of static molecules ( $\sim 43\%$ ) were significantly lower than that observed under non-crowded conditions ( $\sim 70\%$ ), and the estimated clamp opening and clamp closing rates are  $\sim 2$ -fold higher compared to experiments under non-crowded conditions. These results suggest that, in the crowded cellular environment, intrinsic conformational dynamics of the clamp are significantly enhanced, possibly via a relative stabilization of the transition states (Figure 5). We thus suggest that changes in intracellular crowding (e.g. microcompartmentalization due to possible liquid-liquid phase separation; 37) may further alter clamp conformational dynamics and result in modulation of the overall rate of transcription initiation as reported previously (35,36). Future studies monitoring conformational dynamics of RNAP



clamp in live bacterial cells would be important to understand such aspects of transcription regulation.

### Modulation of clamp dynamics during promoter search

Transcription initiation is one of the major targets of gene regulation; part of the regulation may occur via modulation of the process by which RNAP ‘scans’ the bacterial nucleoid to locate and bind to promoter DNA, a process also known as ‘promoter search’. Promoter search has been proposed to occur via either a 3D-diffusion mediated ‘hop and search’ mechanism involving transient binding-unbinding to non-specific DNA, via 1D-diffusion along the bacterial nucleoid involving sliding along non-specific DNA until it encounters a promoter sequence, or via a combination of these processes (25–27). Recent studies tracking single RNAP molecules in single live bacterial cells show that RNAP spends the large majority of its search time (~85%) engaged non-specifically with bacterial nucleoid (38).

It has been hypothesized that the RNAP holoenzyme mainly adopts an open-clamp conformational state, and only transiently samples closed-clamp conformational states, when RNAP holoenzyme interacts with non-specific DNA during promoter search (5). Our results argue against this hypothesis. We find that RNAP holoenzyme mainly adopts a *closed-clamp* conformational state—with slow transitions between closed, partly closed, and open states—when RNAP holoenzyme interacts with non-specific DNA (Figure 5). However, although our results argue against the proposal of a mostly open clamp RNAP molecule sliding along the genomic DNA with transient clamp closures punctuating the promoter search process, the observation that some slow clamp opening-closing transitions do take place when bound to non-specific DNA, raises the possibility that clamp conformational dynamics may play a role during promoter search process. Recent studies combining single-molecule fluorescence measurements with optical tweezers have been able to observe long range 1D-sliding of RNAP molecules on doubly tethered  $\lambda$  DNA (39). A combination of methods used in the aforementioned study with reagents developed here should enable us to capture clamp conformations of actively diffusing RNAP molecules along DNA and provide more mechanistic detail about the role of clamp dynamics during facilitated diffusion of RNAP.

### DATA AVAILABILITY

All our time-trace data are available to anyone upon request. MATLAB software packages TwoTone and ebFRET are available at <https://github.com/annawang692/TwoTone2018> and on <http://ebfret.github.io/>.

### SUPPLEMENTARY DATA

[Supplementary Data](#) are available at NAR Online.

### ACKNOWLEDGEMENTS

The illustrations in Figures 1A, B, 3C, 4C and 5 were created using Biorender.com.

*Author contributions:* A.N.K., R.H.E. and A.M conceived the project; A.M. prepared and characterized protein samples; A.M. and A.W. performed single-molecule experiments; A.M. and A.W. analysed data; A.W. and H.U. performed simulations; A.M. and A.W. prepared figures; and A.M., R.H.E. and A.N.K wrote the manuscript.

### FUNDING

Wellcome Trust [110164/Z/15/Z to A.N.K.]; NIH [GM041376 to R.H.E.]. Funding for open access charge: Wellcome Trust [110164/Z/15/Z].

*Conflict of interest statement.* None declared.

### REFERENCES

- Ebright,R.H., Werner,F. and Zhang,X. (2019) RNA polymerase reaches 60: transcription initiation, elongation, termination, and regulation in prokaryotes. *J. Mol. Biol.*, **431**, 3945–3946.
- Mazumder,A. and Kapanidis,A.N. (2019) Recent advances in understanding sigma70-dependent transcription initiation mechanisms. *J. Mol. Biol.*, **431**, 3947–3959.
- Mandelkern,M., Elias,J.G., Eden,D. and Crothers,D.M. (1981) The dimensions of DNA in solution. *J. Mol. Biol.*, **152**, 153–161.
- Bae,B., Feklistov,A., Lass-Napiorkowska,A., Landick,R. and Darst,S.A. (2015) Structure of a bacterial RNA polymerase holoenzyme open promoter complex. *Elife*, **4**, e08504.
- Feklistov,A., Bae,B., Hauver,J., Lass-Napiorkowska,A., Kalesse,M., Glaus,F., Altmann,K.H., Heyduk,T., Landick,R. and Darst,S.A. (2017) RNA polymerase motions during promoter melting. *Science*, **356**, 863–866.
- Zhang,Y., Feng,Y., Chatterjee,S., Tuske,S., Ho,M.X., Arnold,E. and Ebright,R.H. (2012) Structural basis of transcription initiation. *Science*, **338**, 1076–1080.
- Murakami,K.S. (2015) Structural biology of bacterial RNA polymerase. *Biomolecules*, **5**, 848–864.
- Zhang,G., Campbell,E.A., Minakhin,L., Richter,C., Severinov,K. and Darst,S.A. (1999) Crystal structure of thermus aquaticus core RNA polymerase at 3.3 Å resolution. *Cell*, **98**, 811–824.
- Glyde,R., Ye,F., Jovanovic,M., Kotta-Loizou,I., Buck,M. and Zhang,X. (2018) Structures of bacterial RNA polymerase complexes reveal the mechanism of DNA loading and transcription initiation. *Mol. Cell*, **70**, 1111–1120.
- Weixlbaumer,A., Leon,K., Landick,R. and Darst,S.A. (2013) Structural basis of transcriptional pausing in bacteria. *Cell*, **152**, 431–441.
- Hein,P.P., Kolb,K.E., Windgassen,T., Bellecourt,M.J., Darst,S.A., Mooney,R.A. and Landick,R. (2014) RNA polymerase pausing and nascent-RNA structure formation are linked through clamp-domain movement. *Nat. Struct. Mol. Biol.*, **21**, 794–802.
- Bellecourt,M.J., Ray-Soni,A., Harwig,A., Mooney,R.A. and Landick,R. (2019) RNA polymerase clamp movement aids dissociation from DNA but is not required for RNA release at intrinsic terminators. *J. Mol. Biol.*, **431**, 696–713.
- Chakraborty,A., Wang,D., Ebright,Y.W., Korlann,Y., Kortkhonjia,E., Kim,T., Chowdhury,S., Wigneshweraraj,S., Irschik,H., Jansen,R. *et al.* (2012) Opening and closing of the bacterial RNA polymerase clamp. *Science*, **337**, 591–595.
- Chakraborty,A., Mazumder,A., Lin,M., Hasemeyer,A., Xu,Q., Wang,D., Ebright,Y.W. and Ebright,R.H. (2015) Site-specific incorporation of probes into RNA polymerase by unnatural-amino-acid mutagenesis and Staudinger-Bertozzi ligation. *Methods Mol. Biol.*, **1276**, 101–131.
- Duchi,D., Mazumder,A., Malinen,A.M., Ebright,R.H. and Kapanidis,A.N. (2018) The RNA polymerase clamp interconverts dynamically among three states and is stabilized in a partly closed state by ppGpp. *Nucleic Acids Res.*, **46**, 7284–7295.
- Lin,W., Das,K., Degen,D., Mazumder,A., Duchi,D., Wang,D., Ebright,Y.W., Ebright,R.Y., Sineva,E., Gigliotti,M. *et al.* (2018) Structural basis of transcription inhibition by Fidaxomicin (Lipiamycin A3). *Mol. Cell*, **70**, 60–71.

17. Holden, S.J., Uphoff, S., Hohlbein, J., Yadin, D., Le Reste, L., Britton, O.J. and Kapanidis, A.N. (2010) Defining the limits of single-molecule FRET resolution in TIRF microscopy. *Biophys. J.*, **99**, 3102–3111.
18. Uphoff, S., Holden, S.J., Le Reste, L., Periz, J., van de Linde, S., Heilemann, M. and Kapanidis, A.N. (2010) Monitoring multiple distances within a single molecule using switchable FRET. *Nat. Methods*, **7**, 831–836.
19. Van de Meent, J.W., Bronson, J.E., Wiggins, C.H. and Gonzalez, R.L. Jr (2014) Empirical Bayes methods enable advanced population-level analyses of single-molecule FRET experiments. *Biophys. J.*, **106**, 1327–1337.
20. Zimmerman, S.B. (1993) Macromolecular crowding effects on macromolecular interactions: some implications for genome structure and function. *Biochim. Biophys. Acta*, **1216**, 175–185.
21. Zimmerman, S.B. and Minton, A.P. (1993) Macromolecular crowding: biochemical, biophysical, and physiological consequences. *Annu. Rev. Biophys. Biomol. Struct.*, **22**, 27–65.
22. Christiansen, A., Wang, Q., Cheung, M.S. and Wittung-Stafshede, P. (2013) Effects of macromolecular crowding agents on protein folding in vitro and in silico. *Biophys. Rev.*, **5**, 137–145.
23. Elcock, A.H. (2010) Models of macromolecular crowding effects and the need for quantitative comparisons with experiment. *Curr. Opin. Struct. Biol.*, **20**, 196–206.
24. Zhou, H.X., Rivas, G. and Minton, A.P. (2008) Macromolecular crowding and confinement: biochemical, biophysical, and potential physiological consequences. *Annu. Rev. Biophys.*, **37**, 375–397.
25. Berg, O.G., Winter, R.B. and von Hippel, P.H. (1981) Diffusion-driven mechanisms of protein translocation on nucleic acids. 1. Models and theory. *Biochemistry*, **20**, 6929–6948.
26. Guthold, M., Zhu, X., Rivetti, C., Yang, G., Thomson, N.H., Kasas, S., Hansma, H.G., Smith, B., Hansma, P.K. and Bustamante, C. (1999) Direct observation of one-dimensional diffusion and transcription by *Escherichia coli* RNA polymerase. *Biophys. J.*, **77**, 2284–2294.
27. Wang, F., Redding, S., Finkelstein, I.J., Gorman, J., Reichman, D.R. and Greene, E.C. (2013) The promoter-search mechanism of *Escherichia coli* RNA polymerase is dominated by three-dimensional diffusion. *Nat. Struct. Mol. Biol.*, **20**, 174–181.
28. Roe, J.H. and Record, M.T. Jr (1985) Regulation of the kinetics of the interaction of *Escherichia coli* RNA polymerase with the lambda PR promoter by salt concentration. *Biochemistry*, **24**, 4721–4726.
29. Lozinski, T. and Wierzbowski, K.L. (2009) Evaluation of mixed-salt effects on thermodynamic and kinetic parameters of RNA polymerase-promoter DNA complexes in terms of equivalent salt concentrations. General applicability to DNA complexes. *Acta Biochim. Pol.*, **56**, 695–702.
30. Lozinski, T., Bolewska, K. and Wierzbowski, K.L. (2009) Equivalence of Mg<sup>2+</sup> and Na<sup>+</sup> ions in salt dependence of the equilibrium binding and dissociation rate constants of *Escherichia coli* RNA polymerase open complex. *Biophys. Chem.*, **142**, 65–75.
31. Theillet, F.X., Binolfi, A., Frembgen-Kesner, T., Hingorani, K., Sarkar, M., Kyne, C., Li, C., Crowley, P.B., Gierasch, L., Pielak, G.J. et al. (2014) Physicochemical properties of cells and their effects on intrinsically disordered proteins (IDPs). *Chem. Rev.*, **114**, 6661–6714.
32. Moncany, M.L. and Kellenberger, E. (1981) High magnesium content of *Escherichia coli* B. *Experientia*, **37**, 846–847.
33. Outten, C.E. and O'Halloran, T.V. (2001) Femtomolar sensitivity of metalloregulatory proteins controlling zinc homeostasis. *Science*, **292**, 2488–2492.
34. Lee, D.D., Galera-Laporta, L., Bialecka-Fornal, M., Moon, E.C., Shen, Z., Briggs, S.P., Garcia-Ojalvo, J. and Süel, G.M. (2019) Magnesium flux modulates ribosomes to increase bacterial survival. *Cell*, **177**, 352–360.
35. Sokolova, E., Spruijt, E., Hansen, M.M.K., Dubuc, E., Groen, J., Chokkalingam, V., Piruska, A., Heus, H. A. and Huck, W.T.S. (2019) Enhanced transcription rates in membrane-free protocells formed by coacervation of cell lysate. *Proc. Natl. Acad. Sci. U.S.A.*, **110**, 11692–11697.
36. Ge, X., Luo, D. and Xu, J. (2011) Cell-free protein expression under macromolecular crowding conditions. *PLoS One*, **6**, e28707.
37. Ladouceur, A., Parmar, B.S., Biedzinski, S., Wall, J., Tope, S.J., Cohn, D., Kim, A., Soubry, N., Rodrigo Reyes-Lamothe, R. and Weber, S.C. (2020) Clusters of bacterial RNA polymerase are biomolecular condensates that assemble through liquid–liquid phase separation. *Proc. Natl. Acad. Sci. U.S.A.*, **117**, 18540–18549.
38. Stracy, M., Lesterlin, C., Garza de Leon, F., Uphoff, S., Zawadzki, P. and Kapanidis, A.N. (2015) Live-cell superresolution microscopy reveals the organization of RNA polymerase in the bacterial nucleoid. *Proc Natl Acad Sci U.S.A.*, **112**, E4390–E4399.
39. Heller, I., Marchetti, M., Mazumder, A., Chakraborty, A., Malinowska, A.M., Roos, W., Ebricht, R.H., Peterman, E.J.G. and Wuite, G.J.L. (2018) One-dimensional sliding assists  $\sigma 70$  - dependent promoter binding by *Escherichia coli* RNA polymerase. bioRxiv doi: <https://doi.org/10.1101/494534>, 13 December 2018, preprint: not peer reviewed.